Chinese Chemical Letters 32 (2021) 184–189

Contents lists available at ScienceDirect

Chinese Chemical Letters

journal homepage: www.elsevier.com/locate/cclet

Communication

Phenylenediamine-formaldehyde chemistry derived N-doped hollow carbon spheres for high-energy-density supercapacitors

Ming Xu, Yuheng Liu, Qiang Yu, Shihao Feng, Liang Zhou*, Liqiang Mai*

State Key Laboratory of Advanced Technology for Materials Synthesis and Processing, Wuhan University of Technology, Wuhan 430070, China

ARTICLE INFO

Article history:
Received 22 June 2020
Received in revised form 5 August 2020
Accepted 2 November 2020
Available online 4 November 2020

Keywords:
Porous carbon spheres
Hollow structure
Supercapacitors
Ionic electrolyte
Energy density

ABSTRACT

Porous carbon spheres represent an ideal family of electrode materials for supercapacitors because of the high surface area, ideal conductivity, negligible aggregation, and ability to achieve space efficient packing. However, the development of new synthetic methods towards porous carbon spheres still remains a great challenge. Herein, N-doped hollow carbon spheres with an ultrahigh surface area of 2044 m^2/g have been designed based on the phenylenediamine-formaldehyde chemistry. When applied in symmetric supercapacitors with ionic electrolyte ($EMIBF_4$), the obtained N-doped hollow carbon spheres demonstrate a high capacitance of 234 F/g, affording an ultrahigh energy density of 114.8 Wh/kg. Excellent cycling stability has also been achieved. The impressive capacitive performances make the phenylenediamine-formaldehyde resin derived N-doped carbon a promising candidate electrode material for supercapacitors.

Supercapacitors are well-known safe and reliable energy storage devices. Based on ion adsorption/desorption, they can realize fast energy storage in seconds, subsequently leading to considerable power density (>10 kW/kg) and long lifespan (>10^5 cycles) [1–4]. With these capabilities, supercapacitors occupy an indispensable region in energy storage field such as consumer electronics and low-emission hybrid electric vehicles [2]. Nevertheless, the pervasive application of current supercapacitors has still been constrained by its relatively low energy density (~5 Wh/kg) compared with secondary batteries [2,3].

Porous carbons are the electrode material of choice for supercapacitors. Various porous carbon materials have been explored in supercapacitors, including traditional activated carbons [5], mesoporous carbons [6], carbon nanotubes [7], carbon nanofibers [8–11], graphene [12,13] and carbon spheres [14,15]. Compared to other carbon materials, the porous carbon spheres manifest specific merit in achieving high packing density and thus high volumetric capacitance.

It has long been demonstrated that hetero-atom doping in porous carbons can lead to enhancement in capacitive performance. Introducing foreign atoms, such as N, in carbon is able to bring improved electrochemical activity and electrolyte wettability [16]. Generally, two strategies have been adopted to introduce N in porous carbon spheres: (i) post annealing in NH_3 (also-known as post annealing approach) and (ii) choosing appropriate N-containing precursors (also-known as *in-situ* doping approach). As for the *in-situ* doping approach, the N-doped porous carbon spheres are usually obtained through the self-polymerization of dopamine or polymerization of N-containing phenols and formaldehyde [17,18].

Herein, we proposed a facile strategy to synthesize N-doped hollow carbon spheres (NHCSs) based on phenylenediamine-formaldehyde chemistry. The obtained NHCSs possess an ultrahigh surface area of 2044 m^2/g for ion adsorption, a porous shell for effective electrolyte ion diffusion, and a moderate N-doping for conductivity and wettability enhancement. With these highly desirable properties, the NHCSs demonstrate an ultrahigh specific capacitance of 234 F/g and excellent cycling stability in ionic electrolyte. The phenylenediamine-formaldehyde chemistry provides a brand new platform for the construction of N-doped porous carbon materials for high-performance supercapacitors.

For the synthesis of NHCSs, 0.26 g cetyltrimethyl ammonium bromide (CTAB) and 0.2 g *m*-phenylenediamine (*m*PD) were first dissolved into a mixture of 20 mL deionized water, 4 mL absolute ethanol, and 0.15 mL $NH_3{\cdot}H_2O$. Then, 0.28 mL formaldehyde (37 wt%) was added to initiate the polymerization. After stirring for 20 min, 0.46 mL tetraethylorthosilicate (TEOS) was added into the above solution followed by continuous stirring for 24 h at 25 °C. The resin/SiO_2 composite spheres were collected by centrifugation,

* Corresponding authors.
E-mail addresses: liangzhou@whut.edu.cn (L. Zhou), mlq518@whut.edu.cn (L. Mai).

https://doi.org/10.1016/j.cclet.2020.11.004

washed with water, and dried in oven at 70 °C. Carbon/SiO_2 composite spheres were obtained after carbonization at 800 °C for 5 h in N_2. To remove the silica template, the carbon/SiO_2 composite spheres were dispersed in 4 mol/L NaOH solution and stirred at 60 °C for 12 h. The obtained carbon spheres were then mixed with KOH with a carbon/KOH mass ratio of 1:2, and activated at 700 °C for 1 h in N_2. Finally, NHCSs were obtained after washing the activated sample with dilute 2.0 mol/L HCl. For comparison, *m*-aminophenol was used to replace *m*-phenylenediamine, and the final product was named as NHCSs-APF (APF refers to *m*-aminophenol-formaldehyde).

Scanning electron microscopy (SEM) images were obtained on a JEOL-7100 F microscope at 20 kV. Transmission electron microscopy (TEM) images were collected on a JEM-2100 F microscope at 200 kV. High-angle annular dark-field scanning transmission electron microscopy (HAADF-STEM) images and energy dispersive spectroscopy (EDS) elemental mapping were collected on a Titan G2 60–300 microscope. Nitrogen sorption experiments were performed on a Tristar-3020 instrument at 77 K. Raman spectra were collected *via* a Renishaw InVia micro-Raman spectroscopy system. X-ray diffraction (XRD) measurements were carried out by a D8 Advance X-ray diffractometer with a Cu Kα radiation. X-ray photoelectron spectroscopy (XPS) was carried out on a VG MultiLab 2000 instrument.

For symmetric 2-electrode supercapacitors, the active material: acetylene black:polytetrafluoroethylene (PTFE) ratio in the electrode was 8:1:1. The working electrodes were prepared by pressing the round electrode slices with a mass loading of ~2 mg/cm^2 onto Ni foam. CR2016 type coin cells were assembled in glove box. The ionic liquid and organic electrolytes were $EMIBF_4$ (1-ethyl-3-methylimidazolium tetrafluoroborate) and $TEABF_4$/AN (tetraethylammonium tetrafluoroborate in acetonitrile), respectively. Cellulose membrane (NKK-TF4030) was used to separate two working electrodes. During electrochemical characterization, the electrochemical tests including cyclic voltammetry (CV) and galvanostatic charge-discharge (GCD) were performed on CHI 760E instrument. The cycling stability was tested on LAND system. The gravimetric specific capacitance *C* (F/g) based on the mass of a single electrode in symmetric supercapacitor was calculated from the discharge curve using Eq. 1:

$$C = \frac{2I\Delta t}{mV} \quad (1)$$

where *I* is the constant current (mA), Δt is discharge time (s), *V* (V) is the voltage window (minus *IR* drop) during the discharge process and *m* is the mass of active material in a single electrode.

The energy density *E* (Wh/kg) and power density *P* (W/kg) of the symmetric supercapacitor were calculated by Eqs. 2 and 3, respectively:

$$E = \frac{CV^2}{2 \times 4 \times 3.6} \quad (2)$$

$$P = \frac{3600E}{\Delta t} \quad (3)$$

The synthesis of NHCSs with a hollow porous structure is based on phenylenediamine-formaldehyde chemistry as illustrated in Fig. 1. The *m*-phenylenediamine has two amino groups as electron donors to increase the reaction activity with formaldehyde to form *m*-phenylenediamine-formaldehyde resin. Besides, abundant N doping can be introduced into the final products *in-situ* through the amino groups. As the *m*-phenylenediamine and formaldehyde are added before TEOS, amine-aldehyde resin spheres are quickly formed as the core. The subsequent hydrolysis of TEOS and co-condensation with remaining amine-aldehyde resin leads to the formation of a resin@SiO_2 shell on the resin core, generating the resin/SiO_2 composite spheres. During pyrolysis, the resin@SiO_2 shell acts as a rigid framework to avoid the shrinkage of the particle, while the resin core tends to contract towards the rigid shell at high temperature. As a result, a void can be formed in the centre of carbon/SiO_2 spheres during the pyrolysis process and NHCSs can be formed after NaOH etching and KOH activation.

The detailed morphological feature of the samples is characterized by SEM and TEM. The resin/SiO_2 composite obtained from the sol-gel process shows a uniform spherical morphology with an

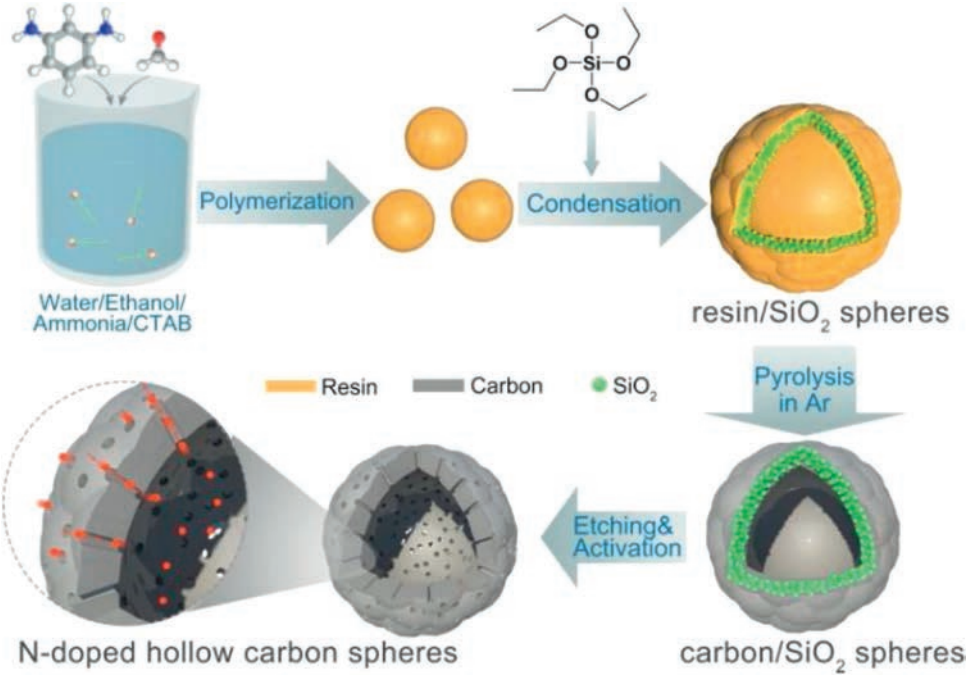

Fig. 1. The synthesis schematic illustration of N-doped hollow carbon spheres.

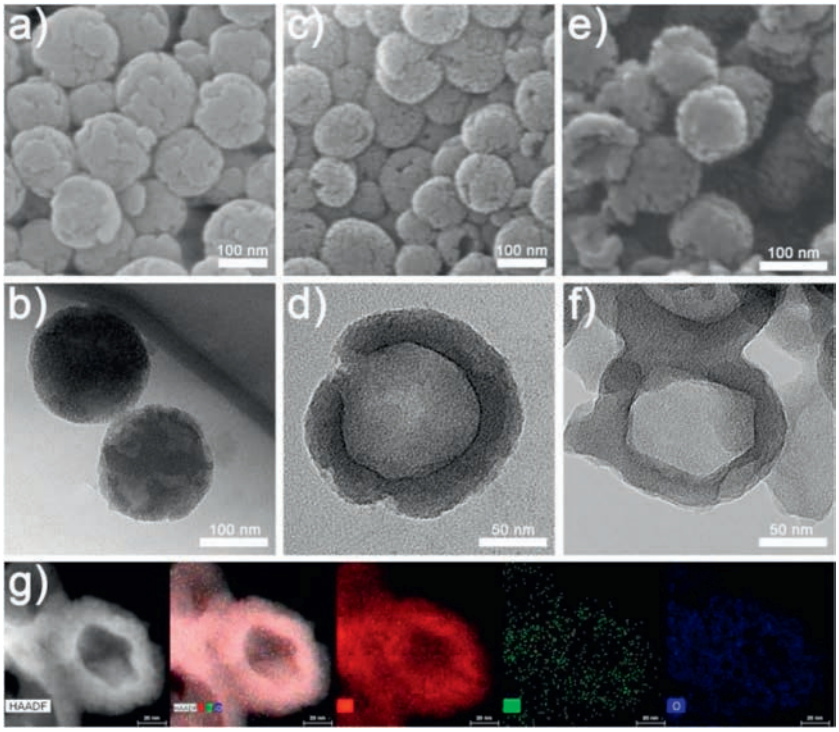

Fig. 2. SEM images of (a) resin/SiO_2, (c) carbon/SiO_2 and (e) NHCSs. (b) TEM images of resin/SiO_2, (d) carbon/SiO_2 and (f) NHCSs. (g) STEM-HAADF image and corresponding EDS elemental mapping of C, N and O of NHCSs.

average diameter of ~150 nm (Figs. 2a and b). EDS elemental mappings demonstrate that the C and N mainly distribute in the core region, while the Si and O mainly distribute in the shell region (Fig. S1 in Supporting information). The EDS results unambiguously demonstrate that the sol-gel derived resin/SiO_2 composite spheres have a resin core and resin@SiO_2 composite shell structure. After carbonization, the obtained carbon/SiO_2 spheres remain the spherical morphology (Fig. 2c) and a hollow cavity is developed in the centre (Fig. 2d and Fig. S2 in Supporting information). The formation of hollow cavity is caused by the outward contraction of resin core towards the relatively rigid resin@SiO_2 shell. After further NaOH etching and activation, NHCSs are obtained although the hollow spherical morphology is partially destroyed (Figs. 2e and f). The average size of NHCSs is ~120 nm, and the cavity size and shell thickness are ~70 and ~25 nm, respectively. N atoms from amino groups have been successfully doped into the carbon framework as evidenced from EDS mappings (Fig. 2g). Graphitic domains can be observed in HRTEM image (Fig. S3 in Supporting information), demonstrating the NHCSs are partially graphitized. The interlayer spacings are measured to be 0.39 nm, much larger than the (002) interlayer spacings of graphite (0.34 nm). It is expected that such partially graphitic carbon would lead to higher conductivity than amorphous carbon. Considering all the structural characteristics, we expected the NHCSs to afford short ion diffusion length and abundant active sites from N-doping for capacitance improvement. By replacing *m*-phenylenediamine with 3-aminophenol, another N-doped hollow carbon sphere sample NHCSs-APF is prepared (Fig. in S4 Supporting information). It is noted that the NHCSs-APF derived from 3-aminophenol present a more uniform size than the NHCSs derived from *m*-phenylenediamine.

XRD was conducted to investigate the crystallinity of the samples. Both the NHCSs derived from phenylenediamine and 3-aminophenol show similar XRD patterns with broad diffraction peaks located at 24° and 43° (Fig. 3a), which is representative for amorphous carbon. N_2 sorption experiments were employed to further study the textural properties of the samples. As shown in Fig. 3b, both isotherms show steep uptake at P/P_0 below 0.05, demonstrating the microporous feature. Besides, the hysteresis at P/P_0 between 0.45 and 1 suggesting the abundant mesoporous characteristic [19]. The surface area of NHCSs is as high as 2044 m^2/g, and that of NHCSs-APF is 1978 m^2/g (Table S3 in Supporting information). The pore size distributions are presented in Fig. 3c. Both samples display abundant micropores below 2 nm and meso-/macropores between 20−70 nm. It is postulated that the meso-/macropores correspond to the hollow cavity, while the micropores may exist in the shell of NHCSs. It has been reported that pores smaller than 0.7 nm is inaccessible and useless for organic electrolyte ions (such as EMI^+ (1-ethyl-3-methylimidazolium)) to provide capacitance [20]. In our case, most of the pores exceed 0.7 nm for both samples. Therefore, it is expected that the NHCSs with ultrahigh surface area, suitable pore size distribution, short mass diffusion length, and effective ion adsorption ability may deliver high electrochemical performance in supercapacitors.

Besides the pore structure, the conductivity is another significant factor influencing the capacitive performance of porous carbons. To investigate the graphitization degree of the samples, Raman spectra were collected (Fig. 3d). The NHCSs and NHCSs-APF feature a broad D band located at 1320 cm^{-1} and a G band at 1587 cm^{-1} [21–23]. The I_D/I_G intensity ratio for NHCSs and NHCSs-APF were 0.94 and 0.96 respectively. The relatively low I_D/I_G ratio (< 1.00) implies a certain degree of graphitization, which may endow the material with a relatively high conductivity. XPS was conducted to investigate the surface chemistry. From the XPS results (Fig. S5 and Table S3 in Supporting information), one can know that the sample derived from *m*-phenylenediamine

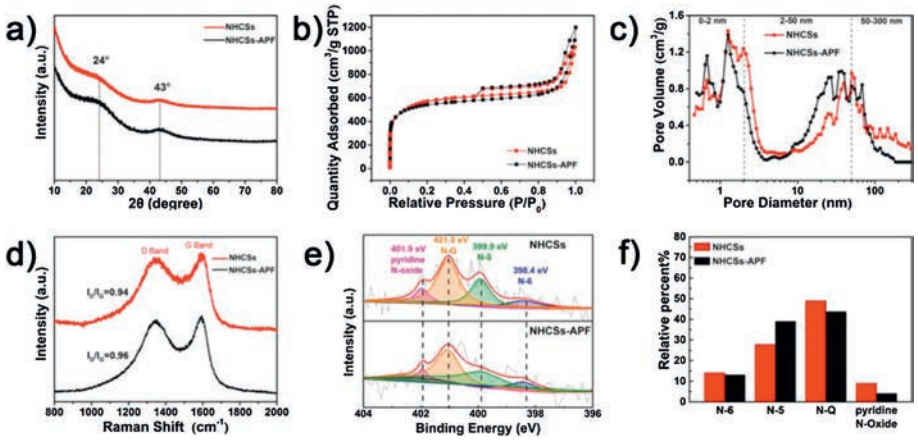

Fig. 3. (a) XRD patterns. (b) N_2 adsorption/desorption isotherms. (c) Pore size distributions. (d) Raman spectra. (e) High resolution N 1s spectra and relative percent of four types of N derived from the (f) XPS spectra.

possesses a slightly higher N content (2.07 at%) than the sample derived from 3-aminophenol (1.58 at%), which is in line with the CHNS elemental analysis (Table S4). A high content of N doping can boost the wettability of electrode materials in electrolytes [24], which is in line with the wettability test, the NHCSs show good wettability in $EMIBF_4$ (Fig. S6 in Supporting information). High-resolution N 1s spectra (Fig. 3e) present four components associated with pyridinic N (398.4 eV), pyrrolic N (399.9 eV), quaternary N (401.0 eV), and pyridine N oxide (401.9 eV). The NHCSs possess a higher fraction of N–Q, which is highly stable and conductive, while the NHCSs-APF show a higher fraction of N5, which is unstable at the elevated voltage (Fig. 3f) [25].

To investigate the electrochemical performance of the samples, symmetric supercapacitors were assembled and tested. Fig. 4 presents the electrochemical properties of NHCSs in $TEABF_4$/AN electrolyte. The CV curves of NHCSs show a larger enclosed area, namely, a higher specific capacitance than those of NHCSs-APF and commercial activated carbon YP-50F (Fig. 4a). The quasi-rectangular shaped CV curves of NHCSs (Fig. 4b and Fig. S7a in Supporting information) demonstrate the typical electric double-layer capacitance storage mechanism. Even at a high scan rate of 500 mV/s, the CV curve exhibits negligible distortion, indicating an extraordinary rate capability resulting from the abundant pores accessible for electrolyte ions as well as the good conductivity for quick response. GCD curves of NHCSs are presented in Fig. 4c. The calculated specific capacitances of NHCSs are 221, 217, 214, 193, 172, 155 F/g at the current densities of 0.5, 1, 2, 5, 10, 20 A/g, respectively. At 0.5 A/g, the NHCSs-APF deliver a much lower capacitance of 167 F/g (Fig. S7b in Supporting information) and commercial YP-50F manifests a capacitance of 117 F/g. In addition, the NHCSs show smaller IR drop in GCD curves (Fig. S8 in Supporting information) and better rate performance (Fig. 4d) than the NHCSs-APF and YP-50F. The cycling performance of NHCSs is shown in Fig. 4e. The NHCSs achieve a good cycling stability, the capacitance retention reaches 84% after 5000 cycles. Benefiting from the abundant active sites, short electrolyte diffusion length, and ideal conductivity, the NHCSs based symmetric supercapacitor achieves a high energy density of 47.7 Wh/kg at 310 W/kg (Fig. 4f), which is significantly higher than those of NHCSs-APF (35.8 Wh/kg) and YP-50F (25 Wh/kg).

When ionic liquid $EMIBF_4$ was employed as the electrolyte, the voltage window can be extended to 3.8 V and the energy density of

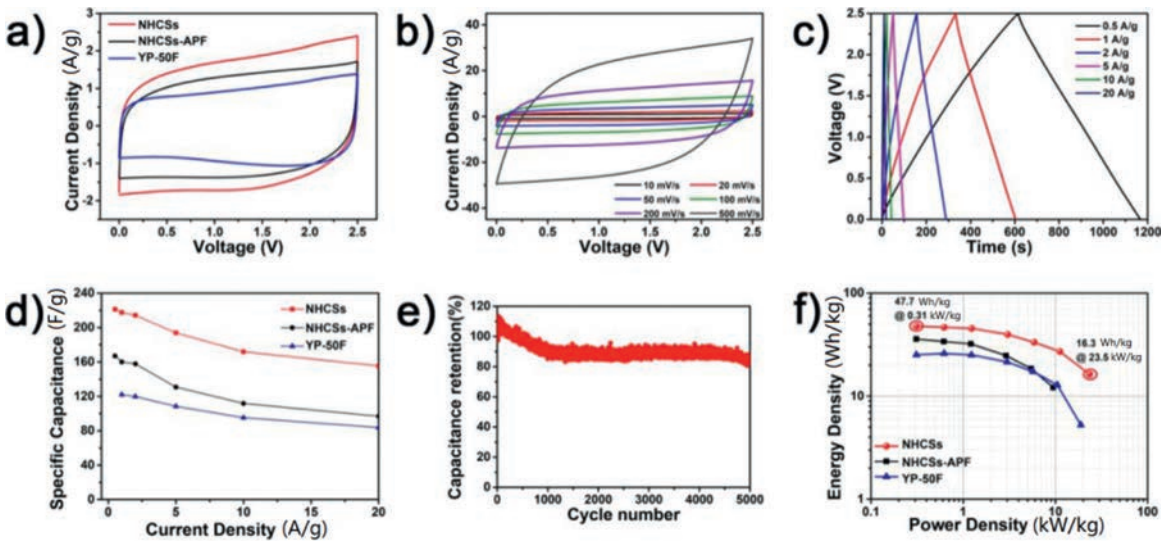

Fig. 4. Supercapacitor performances of NHCSs, NHCSs-APF and YP-50F in $TEABF_4$/AN: (a) CV curves at 20 mV/s; (b) CV curves of NHCSs at different scan rates; (c) GCD curves of NHCSs at different current densities; (d) Rate performances; (e) Cycling performance of NHCSs; (f) Ragon plots.

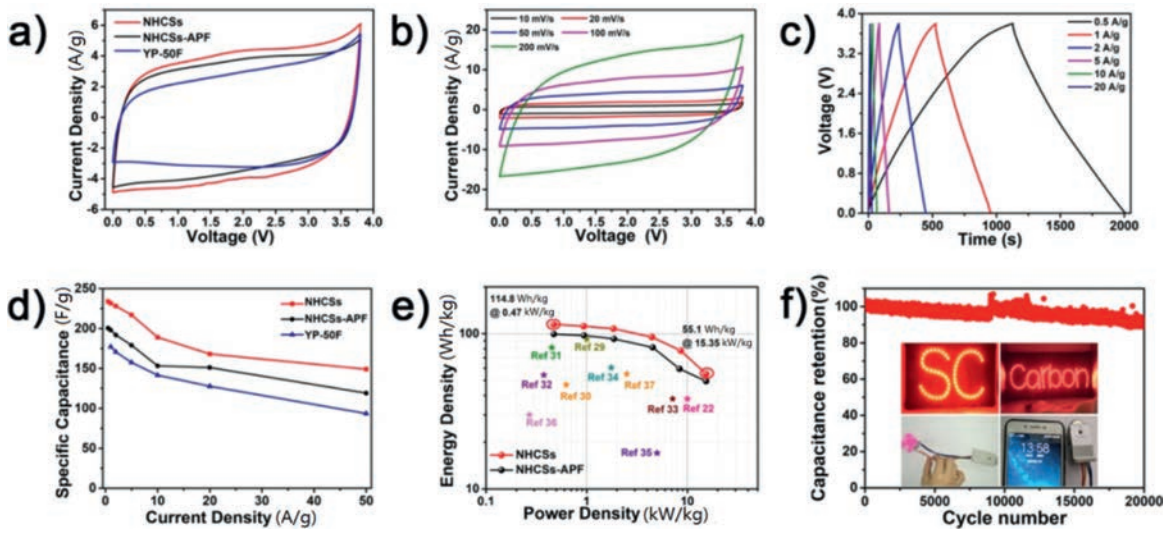

Fig. 5. Supercapacitor performances of NHCSs, NHCSs-APF and YP-50F in $EMIBF_4$: (a) CV curves at 50 mV/s of NHCSs, NHCSs-APF, and YP-50F; (b) CV curves of NHCSs at different scan rates; (c) GCD curves of NHCSs at different current densities; (d) Rate performances of NHCSs, NHCSs-APF, and YP-50F; (e) Ragon plots showing the energy density and power density; (f) Cycling stability of NHCSs and the application of NHCSs based supercapacitors for lighting the LEDs, driving mini fan and charging for smart phones.

symmetric supercapacitors can be further boosted [26–28]. Just like in $TEABF_4$/AN, the NHCSs deliver a higher specific capacitance than NHCSs-APF and commercial YP-50F in $EMIBF_4$ (Fig. 5a). The CV curves of NHCSs also remain *quasi*-rectangular shape (Fig. 5b, Fig. S9a in Supporting information). As indicated from GCD curves (Fig. 5c), the NHCSs deliver a high capacitance of 234 F/g at 0.5 A/g, higher than those of NHCSs-APF (200 F/g, Fig. S9b in Supporting information) and YP-50F (177 F/g). Besides, the NHCSs also demonstrate better rate performance (Fig. 5d) and higher capacitance (Fig. S10 in Supporting information). With a high electrochemical window of 3.8 V, the NHCSs achieve an ultrahigh energy density of 114.8 Wh/kg at 470 W/kg, higher than that of NHCSs-APF (99.4 Wh/kg at 472 W/kg). At 15,350 W/kg, an energy density of 55.1 Wh/kg can be retained (Fig. 5e). To the best of our knowledge, such a high energy density without compromising the power density has far exceeded most porous carbon materials for supercapacitors (Table S5 in Supporting information) [22,29–37]. The performance is also comparable to if not exceeding state-of-the-art supercapacitors based on O/N-doped porous carbons in ionic electrolyte or "water-in-salt" gel electrolyte [38–41]. As an essential parameter for supercapacitor, the cycling stability was also tested. The NHCSs demonstrate a high cycling stability with a capacitance retention of 91% after 20,000 cycles (Fig. 5f). To demonstrate the practical application, the NHCSs were assembled into coin cells. One coin cell (with ~4 mg active materials in total) is able to light 53 and 99 parallel light-emitting diode (LED) lights that assembled into letters "SC" and "Carbon" for more than 60 s, while two coin-cells could drive a mini fan and charge for the smart phone (Fig. 5f inset, and Movies S1–S3 in Supporting information).

Generally speaking, an ideal porous carbon material for supercapacitors should have high surface area, suitable pore size, excellent electrical conductivity, as well as good electrolyte wettability. For the NHCSs synthesized here, KOH activation renders the material an ultrahigh surface area of over 2000 m^2/g. Such a high surface area affords rich active sites for ion adsorption and thus high specific capacitance. The hollow cavity of NHCSs acts as an "ion buffering reservoir" [42–45] while the porous shell ensures short ion transport pathways; both factors are beneficial for the rate capability. In this work, most of the pores in NHCSs exceed the sizes of electrolytes ions ($EMI^+ \approx 0.7$ nm [46], $TEA^+ \approx 0.68$ nm [20]), which further maximize the capacitance [46]. The *in-situ* N-doping provides extra redox active sites for pseudocapacitance and enhances the wettability to electrolytes. At last, the high conductivity of NHCSs further boosts the charge transfer.

In conclusion, N-doped hollow carbon spheres were successfully fabricated based on phenylenediamine-formaldehyde chemistry. With ultrahigh surface area, suitable pore size, moderate N-doping, and high conductivity, the obtained NHCSs demonstrate ideal capacitive performances in supercapacitors. In ionic liquid electrolyte ($EMIBF_4$), the NHCSs achieve a high specific capacitance of 234 F/g and the symmetric supercapacitor delivers an ultrahigh energy density of 114.8 Wh/kg. It is expected that the phenylenediamine-formaldehyde chemistry is a versatile platform for constructing N-doped porous carbons for various applications.

Declaration of competing interest

The authors report no declarations of interest.

Acknowledgments

Ming Xu and Yuheng Liu contribute equally to the article. This work was supported by the National Natural Science Foundation of China (Nos. 21805219, 51521001), the National Key Research and Development Program of China (No. 2016YFA0202603), the Program of Introducing Talents of Discipline to Universities (No. B17034), the Yellow Crane Talent (Science & Technology) Program of Wuhan City.

Appendix A. Supplementary data

Supplementary material related to this article can be found, in the online version, at doi:https://doi.org/10.1016/j.cclet.2020.11.004.

References

[1] P. Simon, Y. Gogotsi, Nat. Mater. 7 (2008) 845–854.
[2] L.L. Zhang, X. Zhao, Chem. Soc. Rev. 38 (2009) 2520–2531.
[3] P. Simon, Y. Gogotsi, Acc. Chem. Res. 46 (2013) 1094–1103.
[4] M. Xu, Q. Yu, Z. Liu, et al., Nanoscale 10 (2018) 21604–21616.
[5] Y. Zhai, Y. Dou, D. Zhao, et al., Adv. Mater. 23 (2011) 4828–4850.
[6] H. Jiang, J. Ma, C. Li, Adv. Mater. 24 (2012) 4197–4202.
[7] M. Kaempgen, C.K. Chan, J. Ma, Y. Cui, G. Gruner, Nano Lett. 9 (2009) 1872–1876.

[8] Q. Yu, J. Lv, Z. Liu, et al., Sci. Bull. 64 (2019) 1617–1624.
[9] L.F. Chen, Z.H. Huang, H.W. Liang, et al., Energy Environ. Sci. 6 (2013) 3331–3338.
[10] L.F. Chen, Z.H. Huang, H.W. Liang, H.L. Gao, S.H. Yu, Adv. Funct. Mater. 24 (2014) 5104–5111.
[11] Y. Cheng, L. Huang, X. Xiao, et al., Nano Energy 15 (2015) 66–74.
[12] F. Qi, Z. Xia, R. Sun, et al., J. Mater. Chem. A 6 (2018) 14170–14177.
[13] X. Yang, F. Zhang, L. Zhang, et al., Adv. Funct. Mater. 23 (2013) 3353–3360.
[14] G. Shen, X. Sun, H. Zhang, et al., J. Mater. Chem. A 3 (2015) 24041–24048.
[15] S. Feng, Z. Liu, Q. Yu, et al., ACS Appl. Mater. Interfaces 11 (2019) 4011–4016.
[16] Z. Ling, Z. Wang, M. Zhang, et al., Adv. Funct. Mater. 26 (2016) 111–119.
[17] C. Liu, J. Wang, J. Li, et al., ACS Appl. Mater. Interfaces 7 (2015) 18609–18617.
[18] C. Liu, J. Wang, J. Li, et al., ACS Appl. Mater. Interfaces 8 (2016) 7194–7204.
[19] L. Yao, Q. Wu, P. Zhang, et al., Adv. Mater. 30 (2018) 1706054.
[20] J. Chmiola, G. Yushin, Y. Gogotsi, et al., Science 313 (2016) 1760–1763.
[21] X. Cui, Z. Pan, L. Zhang, H. Peng, G. Zheng, Adv. Energy Mater. 7 (2017) 1701456.
[22] L. Feng, K. Wang, X. Zhang, et al., Adv. Funct. Mater. 28 (2018) 1704463.
[23] C. Li, X. Zhang, K. Wang, et al., Adv. Mater. 29 (2017) 1604690.
[24] J. Zhao, H. Lai, Z. Lyu, et al., Adv. Mater. 27 (2015) 3541–3545.
[25] L.S. Zhang, X.Q. Liang, W.G. Song, Z.Y. Wu, Phys. Chem. Chem. Phys. 12 (2010) 12055–12059.
[26] M. Bichat, E. Raymundo-Piñero, F. Béguin, Carbon 48 (2010) 4351–4361.
[27] S. Zheng, Z.S. Wu, S. Wang, et al., Energy Storage Mater. 6 (2017) 70–97.
[28] Z. Yang, J. Tian, Z. Yin, et al., Carbon 141 (2019) 467–480.
[29] J. Li, N. Wang, J. Tian, W. Qian, W. Chu, Adv. Funct. Mater. 28 (2018) 1806153.
[30] N. Guo, M. Li, X. Sun, F. Wang, R. Yang, Green Chem. 19 (2017) 2595–2602.
[31] D. Yu, C. Chen, G. Zhao, et al., ChemSusChem 11 (2018) 1678–1685.
[32] C. Chen, D. Yu, G. Zhao, et al., Nano Energy 27 (2016) 377–389.
[33] B. Duan, X. Gao, X. Yao, et al., Nano Energy 27 (2016) 482–491.
[34] Y. An, Y. Yang, Z. Hu, et al., J. Power Sources 337 (2017) 45–53.
[35] G. Ferrero, A. Fuertes, M. Sevilla, J. Mater. Chem. A 3 (2015) 2914–2923.
[36] Z. Chen, J. Wen, C. Yan, et al., Adv. Energy Mater. 1 (2011) 551–556.
[37] L. Zhang, Y. Zhu, W. Zhao, et al., J. Electroanal. Chem. 818 (2018) 51–57.
[38] Z. Song, L. Miao, L. Li, et al., J. Mater. Chem. A 8 (2020) 3717–3725.
[39] Z. Song, H. Duan, D. Zhu, et al., J. Mater. Chem. A 7 (2019) 15801–15811.
[40] Z. Zhou, L. Miao, H. Duan, et al., Chin. Chem. Lett. 31 (2020) 1226–1230.
[41] D. Xue, D. Zhu, H. Duan, et al., Chem. Comm. 55 (2019) 11219–11222.
[42] J. Du, L. Liu, Y. Yu, et al., Chin. Chem. Lett. 30 (2019) 1423–1427.
[43] T. Song, H. Zhao, Y. Hu, et al., Chin. Chem. Lett. 30 (2019) 2347–2350.
[44] Q. Yue, J. Li, Y. Zhang, et al., J. Am. Chem. Soc. 139 (2017) 15486–15493.
[45] T. Zhang, B. Huang, A. Elzatahry, et al., ACS Appl. Mater. Interfaces 12 (2020) 17901–17908.
[46] C. Largeot, C. Portet, J. Chmiola, et al., J. Am. Chem. Soc. 130 (2008) 2730–2731.